SCHOOL OF PHYSICS AND ASTRONOMY

YEAR 3 FINAL PROJECT REPORT

SESSION 2018-2019

Name:	Anthony Joshua Owen
Student Number:	[redacted]
Degree Programme:	Mphys F303
Project Title:	N-body modelling of young protostellar systems
Supervisor:	Dr P Clark
Assessor	Prof J Greaves

Declaration:

I have read and understand Appendix 2 in the Student Handbook: "Some advice on the avoidance of plagiarism".

I hereby declare that the attached report is exclusively my own work, that no part of the work has previously been submitted for assessment (although do note that material in "Interim Report" may be re-used in the final "Project Report" as it is considered part of the same assessment), and that I have not knowingly allowed it to be copied by another person.

Abstract

In this paper we attempt to design, create and run an N-body integrator in Python in order to accurately model the chaotic dynamic interactions of protostars within pre-stellar cores in giant molecular gas clouds. In particular, we focus on the effect the filamentary structure present in these molecular clouds has on the formation of binary and triple star systems. By modelling the protostars as rigid bodies in an N-body integrator and recreating both the structure of localised clusters consisting of 3-5 protostars, as well as the overall filamentary structure that the clusters tend to form into, we hope to determine the effects this has on binary formation relative to isolated systems of stars. As part of this, techniques are developed to find, classify, and calculate the orbital parameters of binary systems with a focus on the gravitational potential energy in the systems. The formation of binaries through processes such as fission and fragmentation are not looked at in this paper as all stars are assumed to have reached sufficient core densities so as to be accurately modelled as a single particle.

Contents

Aims and objectives

In this project, our aim is to model the formation of binary stars through dynamic interaction and capture of protostars. We initially generate a series of clusters - each with three to five protostars - distributed so as to mimic the filamentary structure of pre-stellar cores observed in giant molecular clouds.
The clusters are set up to simulate the distribution of protostars found after fragmentation and breakup of the pre-stellar cores; consequently, gaseous contributions and accretion are ignored in the model and a pure N-body simulation is used.
After running a simulation, we then attempt to identify binary systems and collect information about the systems and compare this to observational data about binary stars.

Chapter 1

Background Theory

1.1 Molecular Clouds

The main area of focus for this report is on binary star formation within the filamentary structure of giant molecular clouds (GMCs). It is previously established that GMCs are effectively stellar nurseries and the principle region for star formation within the universe (Shu 1987) and that embedded clusters account for the formation of 70-90% of stars formed in a GMC (C. J. Lada and E. A. Lada 2003). Further, it is found that most stars are present in binary or multiple systems (Batten 1973) leading to the conclusion that analysis on the formation of binary stars can reasonably be attempted by simulating protostar clusters in the filaments of a GMC.

Within a GMC, the mass distribution is non-homogeneous and tends to the formation of filamentary structures (André 2010). Areas of high and low density are present within the filaments and it is the regions of higher density that become clusters of pre-stellar cores. These clusters are found by André et al. to have a prestellar core mass function (CMF) that closely matches the stellar initial mass function (IMF). This can be seen in figure 1. If the relationship between CMF and IMF is taken to be causal rather than coincidental (Goodwin 2007), then as in Goodwin et al. and Batten, we expect to see a high rate of stars forming as part of binary or multiple systems. This is part of the motivation for determining the methods of formation of binary systems - attempted in this paper through N-body simulation.

The collapse of a GMC into clumps, clusters and cores is due to the Jeans instability (Jeans 1919) shown in Eq. (1.1),

$$E_{gravity} + E_{thermal} < 0, \tag{1.1}$$

which states that a region will begin gravitational collapse when $E_{gravity}$ exceeds $E_{thermal}$. Within a GMC there may be many hundreds of Jeans masses and regions within a GMC can begin collapse independently of the larger system. This is one of the reasons for the non-homogeneity of GMCs and allows for the conditions for star formation to be met.

The Jeans criterion can be used to find the Jeans mass M_j (1.2)

$$M_J = \frac{\pi}{6} \frac{c_s^2}{G^{\frac{3}{2}} \rho^{\frac{1}{2}}}, \tag{1.2}$$

where c_s is the sound speed of the gas, and ρ is the density of the enclosed region. Exceeding this value will begin the gravitational collapse of a given region; it is these regions that become clumps and the increased density allows for the formation of dense pre-stellar cores, within which protostars can begin forming.

1.2 Binary Systems

When looking at the formation of binary stars, it is first necessary to determine how a binary system is defined. The main criteria for classification of a two body system is whether the bodies are gravitationally bound. That is to say the total potential energy is greater than the kinetic energy and so neither body can achieve escape from the system. In fact, Eq. (1.1) applies to solid bodies as it does to gas clouds. A negative total energy leads to collapse of a cloud and to gravitational binding for few body systems.

A second criteria is necessary to differentiate between a binary system, a central body with many smaller bodies surrounding it (e.g Saturn's rings) and a body-satellite system. A general approximation will be assumed in this paper that if the centre of mass of the system lies outside of the most massive body in the system, then the system can be classified as a binary. This is not a perfect solution but for the purposes of this paper it will suffice. As an example, the reclassification of Pluto as recently as 2006 illustrates the difficulty in determining the exact conditions to differentiate between a binary system and a body/satellite system. Although Pluto is a dwarf planet in a binary with Charon as opposed to stars/protostars, the logic in determining the nature of the system can be applied.

Now that there is a way to classify what a binary system is, we look towards processes by which they can form. Two formation processes for binary systems are described below; binaries by capture and by fragmentation (Tohline 2002).

Capture describes a system such that stars form within clumps as individual bodies and then by dynamical encounters with either stars from the same clump, or stars external to the clump, form bound pairs. An example of this is a three body interaction where one body is ejected with a significantly greater kinetic energy than it entered with as seen in Fig. 1.1. Conservation of energy means that this energy comes from the other two bodies, leaving them with a lower total energy. If this new two body system has a potential energy greater than the kinetic energy then the two bodies will be gravitationally bound and can be a potential binary system. Because capture requires three bodies to pass close enough together at the same time so as to interact, it is theorised that this is a low frequency occurrence and is unlikely to be the main source of binary star formation (Batten 1973). It is an aim of this project and the simulation to determine if three body dynamic interactions occur with a greater frequency than initially thought. Preliminary tests such as in Fig. 1.1 indicate that this may be the case.

Fragmentation is when a single rotating gas cloud spontaneously separates into two smaller clouds that will proceed to orbit each other (Fig. 1.2). Each cloud

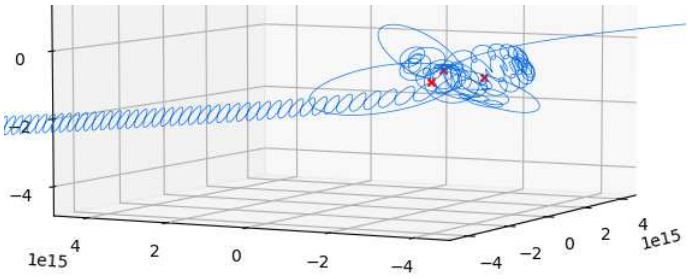

Figure 1.1: An example interaction between three bodies resulting in the ejection of one body and the formation of a bound pair between the remaining bodies. The starting positions are marked with "x".

can then form a pre-stellar core and a binary system will eventually form with the angular momentum coming from the angular momentum of the core and surrounding gaseous material. This fragmentation process can happen during the initial collapse of the GMC, prompt fragmentation; at a later stage, delayed fragmentation; or through collisions of clumps. Prompt fragmentation occurs when the centre of a GMC begins collapsing into a stable equilibrium state. The fragmentation will then occur as the high angular momentum material from the outer edges of the core accretes onto the central high density region and disrupts the equilibrium. This can then lead to the formation of a binary system (Tohline 2002).

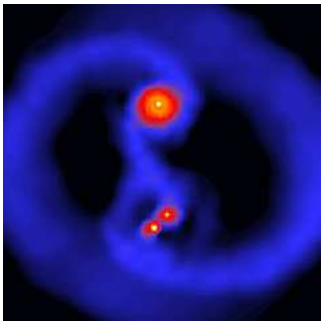

Figure 1.2: An example of the process by which binaries may form through fragmentation. Image credit: Bate, Bonnell, and Price 1995.

Fragmentation by collisions between clumps in a molecular cloud is also worth noting. These collisions generate dense areas which begin to fragment and achieve densities high enough to form protostellar disks. These disks can then interact and form binary systems that lead to binary cores and eventually stars (Turner 1995). The formation of binaries disks in this way leads to an increased probability of dynamic interactions between the cores due to the close proximity and pre-existing interaction between the systems.

Due to the simulation being run as a pure N-body, there is no accounting for gas, accretion, or formation of binaries through fragmentation. Instead, the clusters are initially modelled as being in a stage of evolution after fragmentation has occurred and dense protostars have already formed. These clusters are modified so they are initially bound - as would be the case for a cluster of protostars formed from a single core - and are then evolved in time to examine only the effects of dynamic interaction on further formation of binary systems.

Chapter 2

Simulation

2.1 Integrator scheme

The choice of which numerical integration scheme to use was influenced by three factors: accuracy, complexity, and ease of implementation. The three methods of integration that were considered are:
The simple Euler Eq. (2.1),

$$\begin{aligned} \vec{r}(t+\Delta t) &= \vec{r}(t) + \vec{v}(t)\cdot\Delta t \\ \vec{v}(t+\Delta t) &= \vec{r}(t+\Delta t) + \vec{a}(t)\cdot\Delta t, \end{aligned} \tag{2.1}$$

where $\vec{r}$, $\vec{v}$, and $\vec{a}$ are vectors representing position, velocity and acceleration. The current time step is (t) and the next time step is $(t+\Delta t)$ with Δt being the finite calculation time step used.
The Verlet method (the leapfrog method) Eq. (2.2),

$$\begin{aligned} \vec{r}(t+\Delta t) &= \vec{r}(t) + \vec{v}(t)\cdot\Delta t + \frac{1}{2}\vec{a}(t)\cdot\Delta t^2 \\ &\text{Calculate } \vec{a}(t+\Delta t) \text{ using } \vec{r}(t+\Delta t) \\ \vec{v}(t+\Delta t) &= \vec{v}(t) + \frac{1}{2}(\vec{a}(t)+\vec{a}(t+\Delta t))\cdot\Delta t, \end{aligned} \tag{2.2}$$

and the Runge-Kutta 4th order scheme. The simple Euler scheme is by far the fastest to run and is very simple to implement. However, it is a non-symplectic scheme and so suffers from high inaccuracy and does not conserve the total energy of the system (Fig. 2.1b).

The Runge-Kutta 4th order scheme has the highest computational cost and is also the hardest to implement. For this reason the Verlet method was chosen and implemented. As it is symplectic (it obeys Eq. (2.3),

$$\dot{p} = \frac{\partial H}{\partial q} \quad \text{and} \quad \dot{q} = \frac{\partial H}{\partial p}, \tag{2.3}$$

where H is the Hamiltonian, q and p are the position and momentum coordinates - the Verlet method conserves energy and balances computational complexity with accuracy over long simulations. A comparison of the Euler and Verlet methods can be seen in Fig. 2.1 and Fig. 2.2 respectively.

The most obvious drawback of the Euler integration scheme is that even in this simple binary system, there is a large enough error that, despite the stars starting

in a bound and stable orbit, they experience orbital decay and are both spiralling outwards. This can also be seen in the energy graphs where the Euler system is showing a trend towards increasing total energy. In contrast, the Verlet system, over a large timescale, has a constant total energy (The start and end of the total energy lines exhibit a strange trend. This is due to the total energy being a moving average of 1000 values). The orbits of the stars can also be seen to be stable and not deviating from the initial bound and stable orbit.

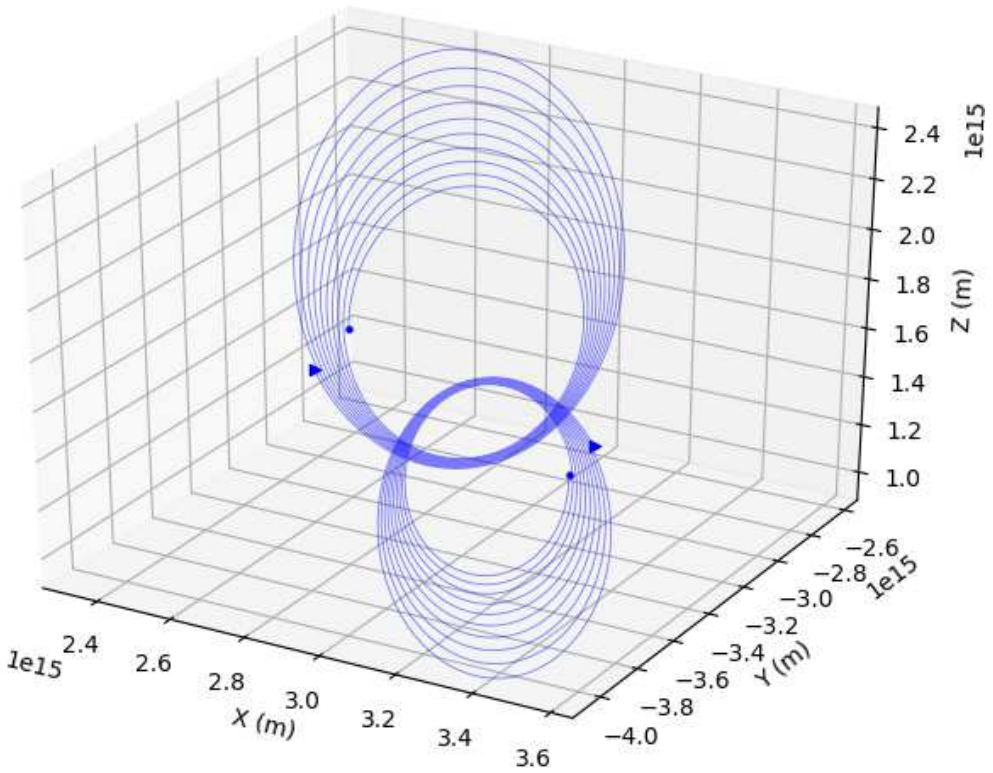

(a) A simple binary system. The starting positions are marked with "o" and the end with and arrow.

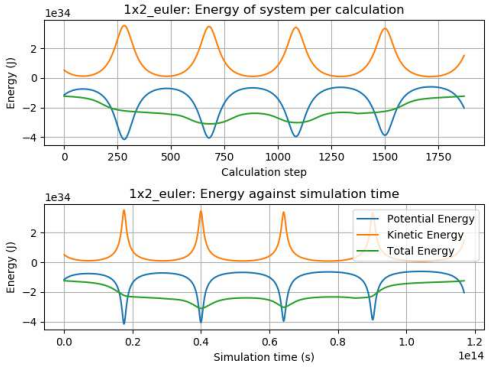

(b) Energy of system.

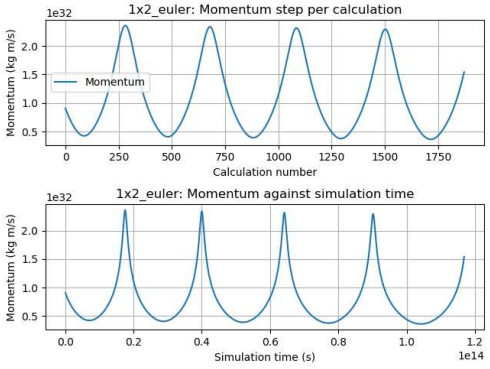

(c) Momentum of system.

Figure 2.1: Euler integration of a simple binary system.

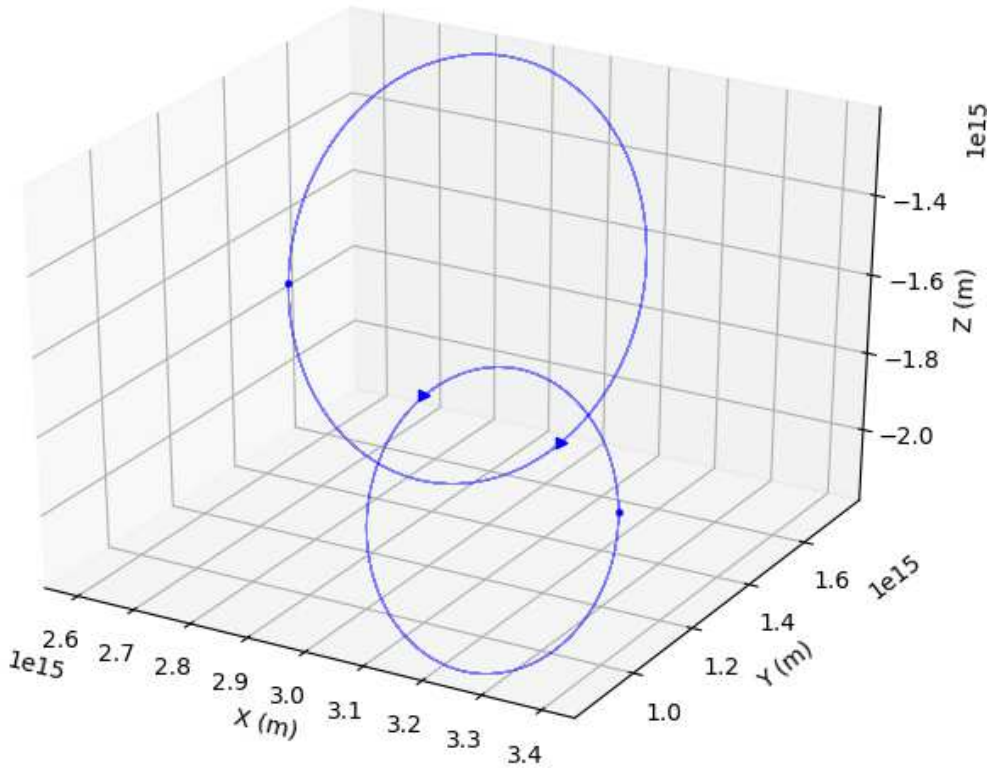

(a) A simple binary system. The starting positions are marked with "o" and the end with and arrow.

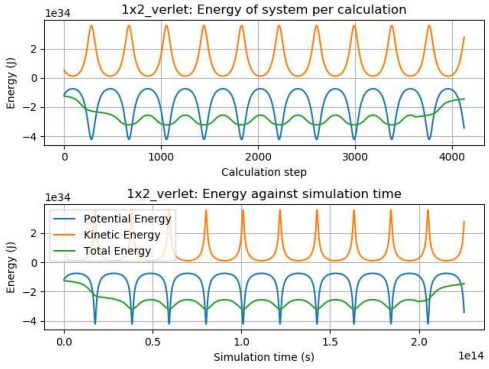

(b) Energy of system.

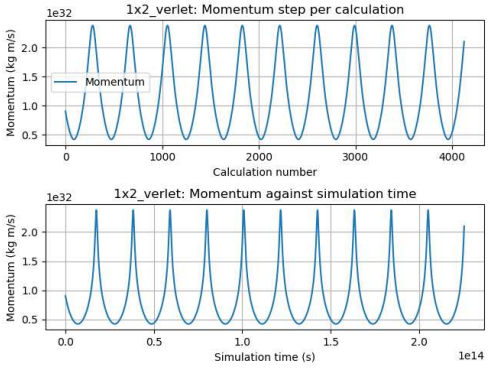

(c) Momentum of system

Figure 2.2: Verlet integration of a simple binary system.

2.2 Code Optimisation

2.2.1 Softening Parameter

When designing and creating the N-body integrator portion of the code, there were two main issues to deal with. Firstly, in the event that two bodies have a close encounter, a divide by zero error can occur in the force calculations (Eq. 2.4). This results in unrealistic behaviour during close encounters and typically presented as the acceleration tending to infinity. The solution is to add a softening parameter, ϵ, in the force calculation Eq. 2.5 (Athanassoula 2000). This has the effect of limiting the minimum effective distance between bodies and so avoids errors from the $\frac{1}{r^2}$ in the calculation,

$$F = -\frac{G \cdot M_1 M_2}{|r|^2}\boldsymbol{r} \tag{2.4}$$

$$F = -\frac{G \cdot M_1 M_2}{(|r|^2 + \epsilon^2)^{\frac{3}{2}}}\boldsymbol{r} \tag{2.5}$$

where $\boldsymbol{r}$ is the relative distance vector between the two bodies in question, M_1 and M_2 are the masses of the bodies, and G is the gravitational constant. The value of ϵ is set to approximately one solar radius. This allows for avoidance of collisions but is not large enough to significantly affect the force calculations for more distant bodies.

2.2.2 Dynamic time stepping

A well known issue with N-body simulators is that the run time is on the order $O(n^2)$. It was not possible to reduce this so instead a dynamic time step solution was implemented as an alternative. A method for reducing run time is to increase the time step increment so that a greater simulation time can be achieved in the same number of calculation cycles. This solution has the significant drawback of a direct correlation to loss of accuracy, particularly during close interactions - a key focus of this simulation. In order to negate this, the time step of the program is instead calculated with respect to the softening parameter, ϵ and the current accelerations of the bodies in the system. The time step for each step was calculated using Eq. 2.6,

$$\delta t = \sqrt{\frac{\mu * \epsilon}{a_{max}}}, \tag{2.6}$$

where μ is a constant and a_{max} is the greatest acceleration of any object at the current time step. The results of this is that the simulation runs using a time step that ensure the fastest accelerating object moves a maximum distance corresponding to the softening parameter. This results in greatly reduced run time whilst maintaining the same level of calculation accuracy.

To test this, the simulation was run with a Sun/Earth/Moon/Mars known system. By using a known system this simulation also serves to show that the dynamic time stepping does not affect the accuracy of the calculations as a stable orbit is predicted by the initial conditions. A slight modification was made by reducing the initial velocity of Mars by 50% to place it in an elliptical orbit. This provided a large contrast between the small and fast acceleration values over the course of the simulation. The values of δt can be seen in Fig. 2.3. In the test simulation,

the addition of dynamic time stepping reduced run time by more than a factor of ten. Given the large computational load, this is a significant improvement and has allowed for future runs to be simulated over a much longer time scale.

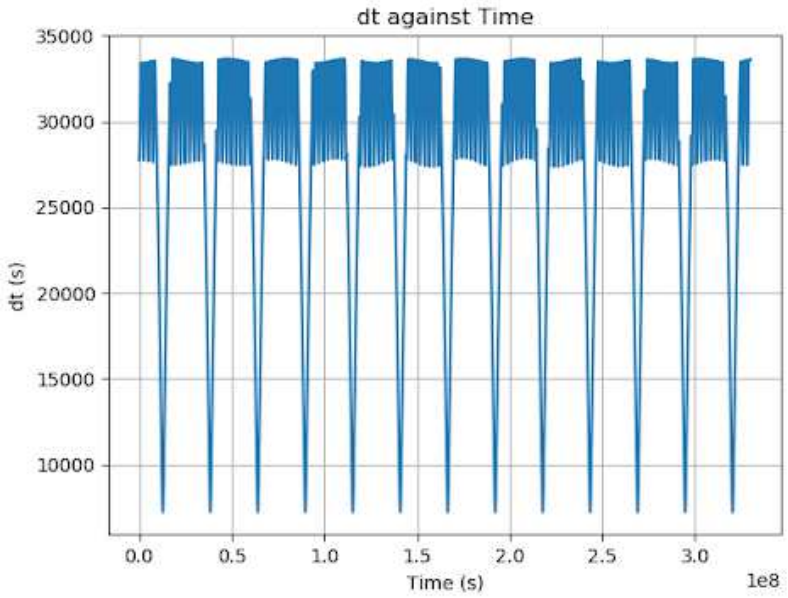

Figure 2.3: The time step per iteration as a function of time (1̃0 years). The repeating minimas' occur when Mars (on an elliptical orbit) passes its perihelion and thus has the highest acceleration. The higher frequency oscillations seen are from the moon/earth system.

2.3 Initial set-up

The aims of the initial set-up portion of the project is to generate a system of bodies that resemble the positions and relative velocities of protostars formed within pre-stellar cores and to arange these clusters in a filament resembling those observed in GMCs. To do this, the following steps were taken:

- Generate a cluster of bodies with no group velocity
- Scale the velocities of the bodies to obey the virial theorem
- Generate a filament of clusters that matches observations of GMCs

The size and scale of the filament is taken from André 2010 and the initial observations of the Herschel Gould belt survey.

2.3.1 Cluster generation

The clusters were generated using a Gaussian distribution centred on $(0, 0, 0)$. The masses are generated in the range 0.1-1.5 solar masses and a random (x, y, z) velocity was added to each body. A sample cluster consisting of 5 bodies can be seen in Fig. 2.4a. The overall velocity of the cluster is automatically calculated and subtracted from each body in order to ensure the cluster is stationary at the start of the simulation.

In order to ensure the clusters are bound clusters, the velocities are scaled after generation according to the virial theorem Eq. (2.7),

$$E_{kinetic} = \frac{-1}{2} E_{potential} \tag{2.7}$$

where E_k, the kinetic energy, is calculated relative to the centre of velocity of the system, and E_p, the potential energy, is the sum of the potentials between all bodies in the system. This ensures that each cluster will interact preferentially within itself before further cluster-cluster interactions take place. Fig. 2.4b illustrates the initial "collapse" of the cluster as expected from scaling the velocities. Three of the five bodies are then ejected and a binary system is formed. This binary has a net velocity, allowing for potential interactions between other clusters in its path. The binary can also be seen in the oscillations of the energy graph (Fig. 2.4c). As the binaries orbit each other they transfer between kinetic and potential energy but the total system energy always averages to a constant value.

The dynamic time stepping (Fig. 2.4d) can also be seen to be working as the initial chaotic start stabilises to a value that ensures the binary pair is calculated without accuracy loss. The strong influence from the formation of a binary pair, and its regular, oscillating accelerations means that the graph of time step against calculation step can be used to determine when a binary forms. This is verified with the binary detection code after the simulation but it does provide a good indicator of the formation time for the binary pair.

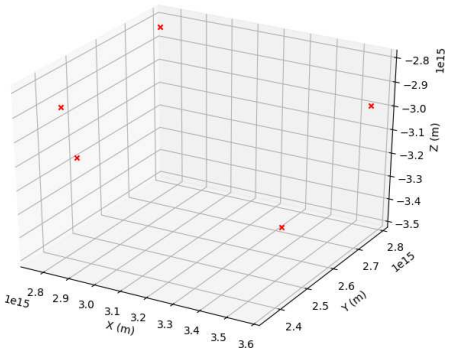

(a) An example of the random generation of a single 5 body cluster.

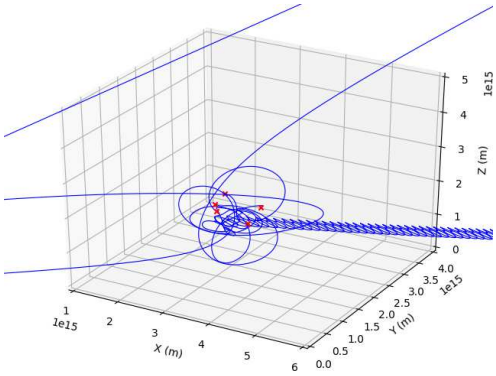

(b) A short simulation of a single cluster of 5 bodies.

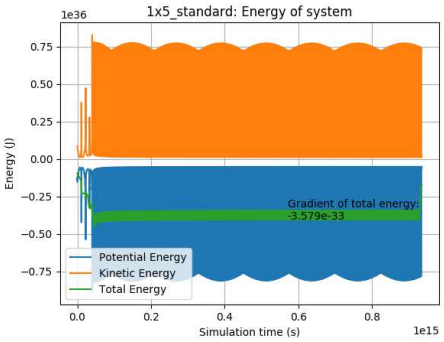

(c)
System energy for a single, five body cluster. Using the Verlet method results in energy conservation over over large timescales.

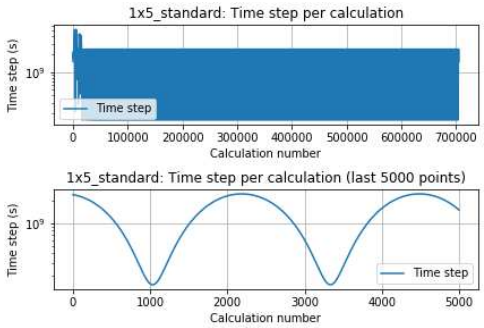

(d) Time step per calculation interval.

Figure 2.4: Single cluster generation and testing. Red "x" are initial positions, Blue line indicate the path of the bodies. The formation of the binary system can be seen at approximately $4 \times 10^{13} s$.

2.3.2 Filament generation

The filamentary structure is generated by placing each cluster incrementally along the x-axis and adding some variation to the y and z axis. By setting each cluster to progress some (x, y, z) distance relative to the previous cluster instead of increments along the x-axis and adding $(const, y, z)$ variation only, it allows for more natural bends and structure variations in the generation whilst still maintaining the overall filamentary structure. The filaments are generated such that the random generation of the full filaments can be see in Fig. 2.5.

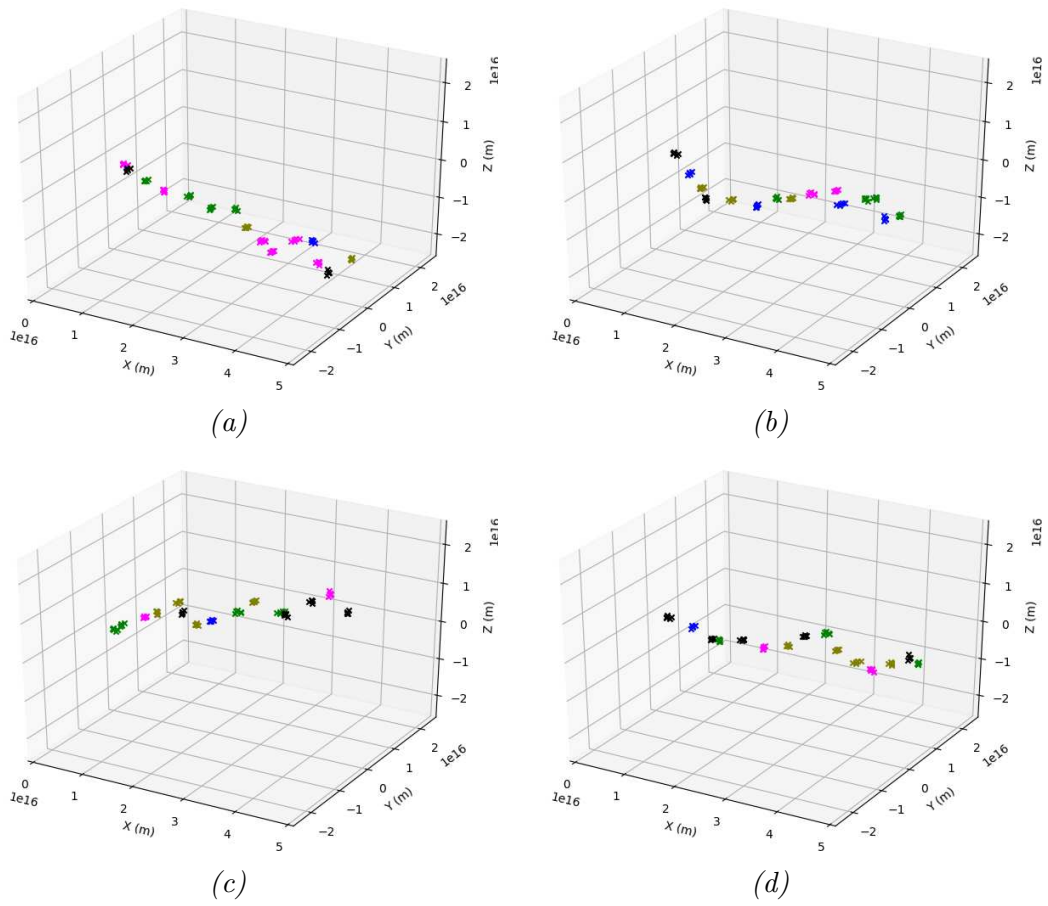

Figure 2.5: Four examples of filaments generated with 15 clusters of three bodies each.
N.B colours are used only to indicate separate clusters in case of overlap due to restricted viewpoint on a 3-D plot.

2.4 Automated binary detection

In order to automatically detect and identify binary systems, the criteria of binary systems having a greater potential energy than other pairs in the system was used. The basic algorithm used for detection is as follows:

1. Calculate the potential energy between every possible pair of bodies
2. Select the pair with the highest potential energy
3. Create a "binary object" that is a combination of the two base bodies
4. Remove the two base bodies from the list of bodies and replace with the new binary object
5. Repeat

The benefit of only selecting the most bound binary each iteration is that it allows for the detection of triple systems as each found binary is included in subsequent calculations. A drawback of this technique is that there is a tendency for a triple system to be detected, this system then has a large enough mass that it becomes the target of the next iteration due to the larger potential energy. This leads to a quadruple system and so on, eventually creating a a single object encapsulating all bodies in the simulation. Due to the way the binaries are tracked, it is fairly simple to see when this effect starts becoming dominant as each further binary detected this way is comprised in part of the previous one. Further iterations of the algorithm can be safely ruled out, leaving only the "true" binary and triple systems in the results. The algorithm was tested and the results initially verified by visual observation as shown in Fig. 2.6.

2.4.1 Orbital parameters of binary systems

The semi-major axis (a) of a binary system was determined using Eq. (2.8),

$$a = -\frac{G \cdot M_1 \cdot M_2}{2(E_k + E_p)}, \tag{2.8}$$

where M_1 and M_2 are the masses of the primary and secondary body in the binary, E_k and E_p are the kinetic and potential energies of the pair respectively. The kinetic energy is calculated by evaluating both bodies energies with respect to the centre of velocity of the two body system, rather than relative to the rest of the bodies.

The mass ratio q of the binary systems is defined as in Eq. (2.9),

$$q = \frac{M_s}{M_p}, \tag{2.9}$$

where M_s and M_p are the secondary and primary masses respectively. The secondary body in a binary is the lower mass of the pair, leading to $q \leq 1$.

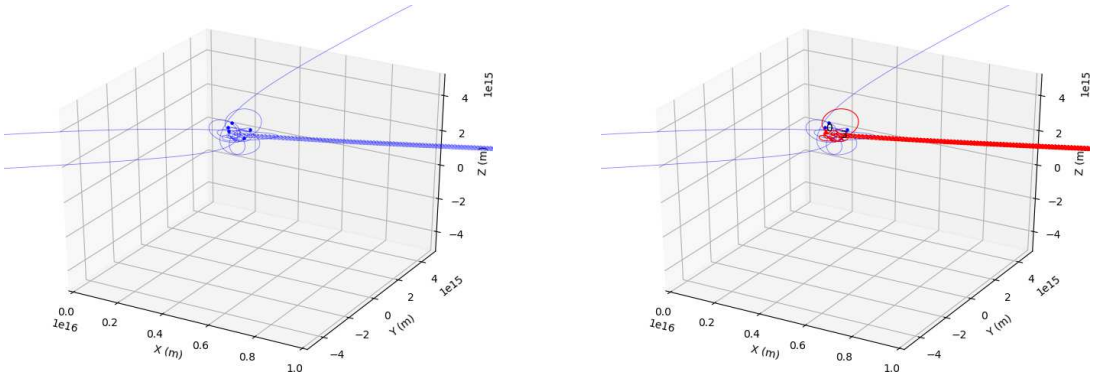

(a) *(b)*

Figure 2.6: A single cluster of five bodies. Automated detection algorithm identified bodies "0", and "3" as binaries - they are shown plotted in red here.
$q = 0.53, \quad a = 1808au$

Chapter 3

Results

3.1 Single cluster

A single cluster of five bodies was chosen as a baseline for ensuring correct cluster self-interaction. The results from three tests with a different random seed can be seen in figures 3.2, 3.3, 3.4. The formation of a binary system (highlighted in red) can be seen as the energy, momentum, and time step all tend to a steady state. The formation of a binary system also means that the simulation continues on at a time step suitable to ensure accuracy of the binaries orbit - forcing a slow down of the whole simulation and greatly increasing run time after the formation of the first binary.

This slow down can also be seen in plots of simulation time against run time. The simulation tends to a power law relationship of the form Eq. (3.1),

$$y = Ax^k, \tag{3.1}$$

where A and k are constants, y is the run time and x the simulation time.
After formation of the binary, this tends to the result of $k = 0.50 - 0.55$. The fit of the plots was calculated using only the data from the second half of the simulation. This is after the main binary system has formed and ensures the power law relates to the time steps affected by the binary and the small time steps associated with it.

Table 3.1: Potential energy of the most bound binary pair.

Run number	Potential energy of most bound pair (J)	k
1	-1.35×10^{38}	0.05
2	-1.95×10^{35}	0.70
3	-1.61×10^{35}	0.52

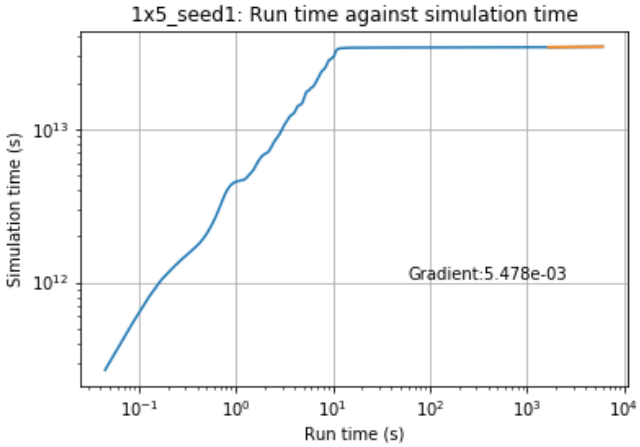

(a) Run 1: $k = 0.005$

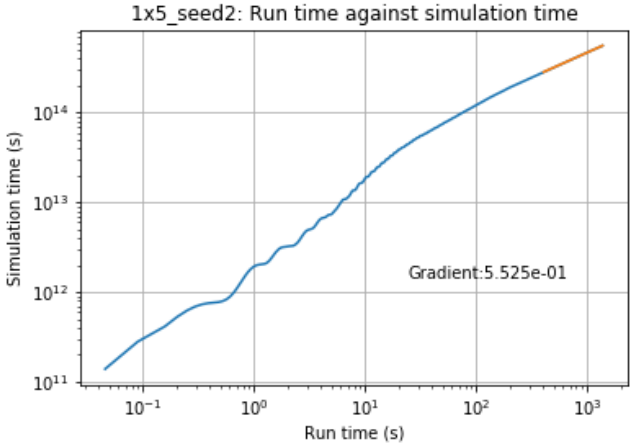

(b) Run 2: $k = 0.55$

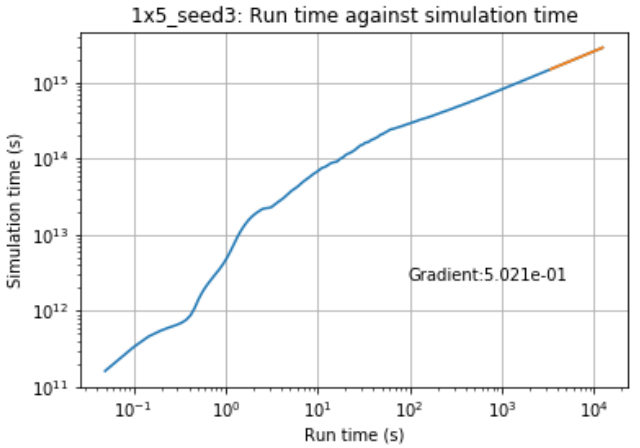

(c) Run 3: $k = 0.50$

Figure 3.1: A log scale plot of simulation time against run time. The formation of a binary can be seen as the graph tending to the form of equation (3.1).

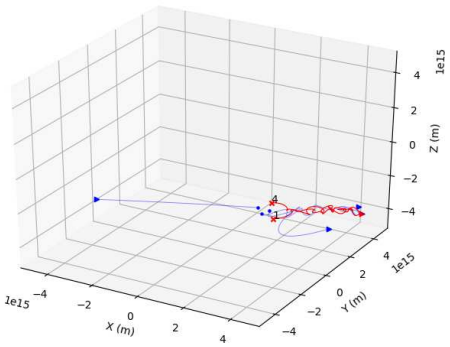

(a) A plot of the positions of the bodies over time. Detected binaries shown in red.

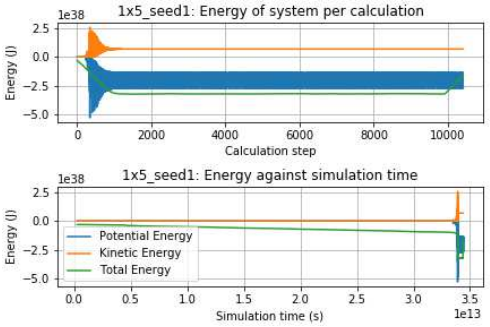

(b) Energy as a function of simulation time and calculation number.

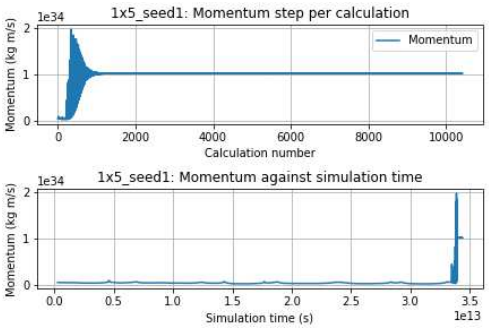

(c) Magnitude of total momentum as a function of simulation time and calculation number.

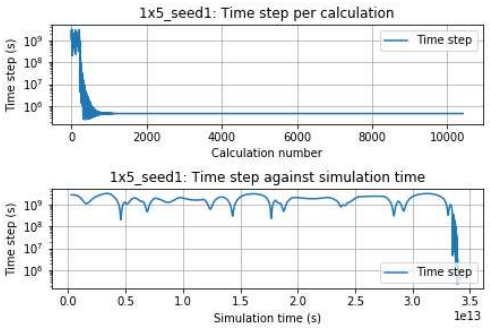

(d) Time step size as a function of simulation time and calculation number.

Figure 3.2: Run 1 of a five body cluster
A tight binary is formed after numerous 3-body interactions. A triple system appears to have formed but the tight binary resulted in very small time steps and so no further evolution of the system was observed. Binary forms at $\sim 3.3\times10^{13}$.

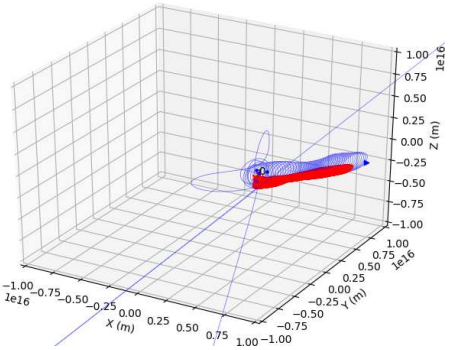

(a) A plot of the positions of the bodies over time. Detected binaries shown in red.

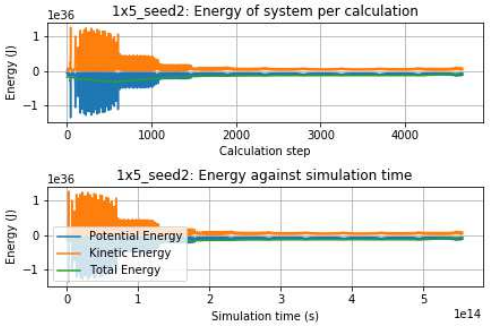

(b) Energy as a function of simulation time and calculation number.

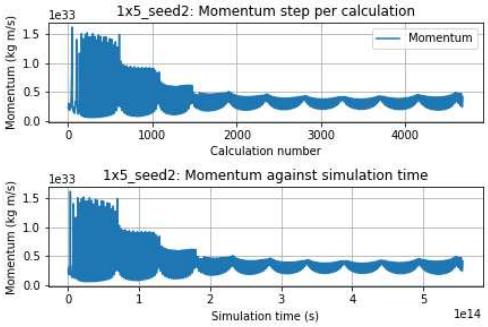

(c) Magnitude of total momentum as a function of simulation time and calculation number.

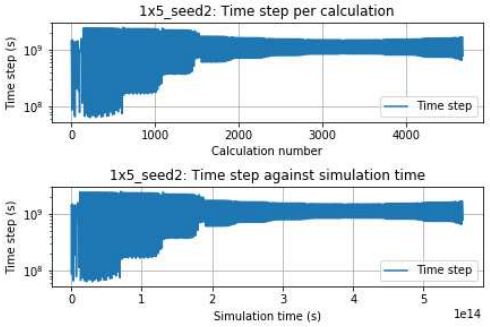

(d) Time step size as a function of simulation time and calculation number.

Figure 3.3: Run 2 of a five body cluster
A stable triple system can be seen. A binary is initially formed and several further interactions can be seen eventually forming a triple system. Triple forms and stabilises at $\sim 2 \times 10^{14}$.

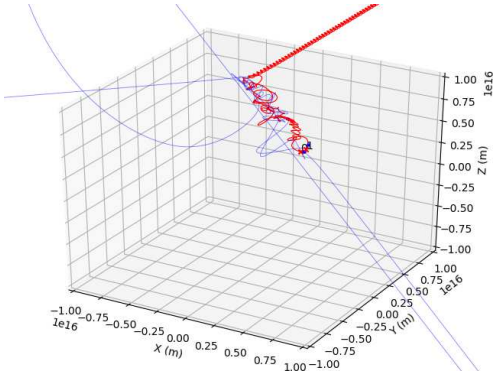

(a) A plot of the positions of the bodies over time. Detected binaries shown in red.

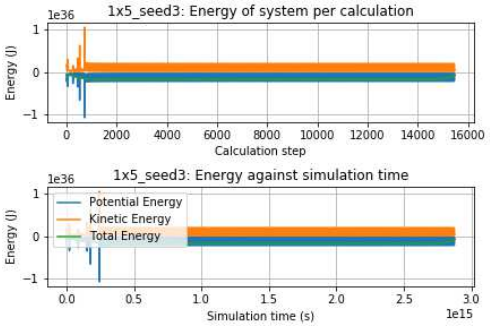

(b) Energy as a function of simulation time and calculation number.

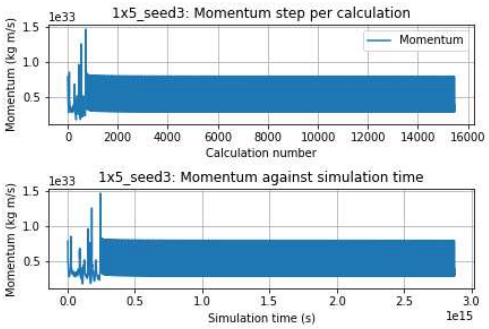

(c) Magnitude of total momentum as a function of simulation time and calculation number.

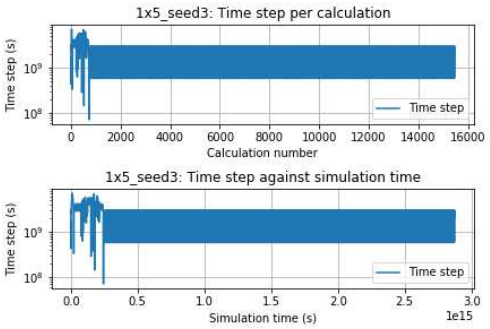

(d) Time step size as a function of simulation time and calculation number.

Figure 3.4: Run 3 of a five body cluster
A binary is seen to form from a chaotic and long lasting initial interaction. The binary is ejected from the system shortly after formation. Binary forms at $\sim 2.5 \times 10^{14}$.

3.2 Filaments

Simulations were run with clusters of three stars and filaments comprised of 3 to 6 clusters. Ideally the clusters would be made up of five stars each but due to time constraints and the run time with n^2 as more bodies are added to the simulation, three was determined as an ideal balance between having enough stars for an initial interaction between clusters whilst having enough clusters for inter-cluster interaction - whilst still keeping the total body count at less than 20.

A 3x3 (3 clusters of 3 bodies, Fig. 3.5) simulation was used as a baseline for the minimum number of clusters and bodies. A 3x4 (3 clusters of 4 bodies) is shown in Fig. 3.6.

Binary stars were positively identified in eight runs of a single five body cluster as well as in a run of three clusters of three bodies, and a run of three clusters of four bodies. A plot of the semi-major axis of these binaries against the potential energies is shown in Fig. 3.7

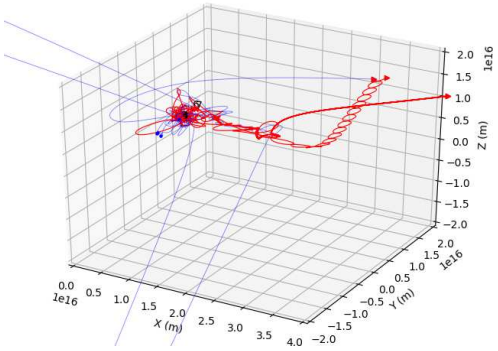

(a) A plot of the positions of the bodies over time. Detected binaries shown in red.

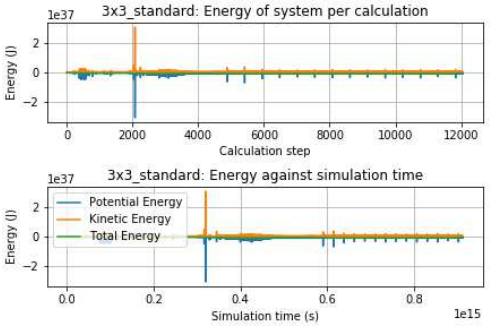

(b) Energy as a function of simulation time and calculation number.

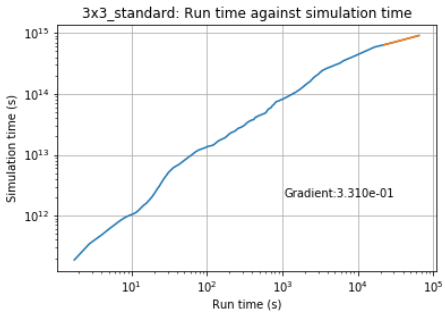

(c) A log log plot of simulation time against runtime. The last half of the data is used to plot the fit (shown in orange).

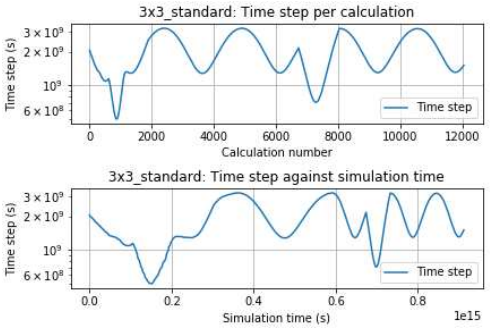

(d) Time step size as a function of simulation time and calculation number.

Figure 3.5: Cluster size = 3, Number of clusters = 3, binary pairs formed = 2.

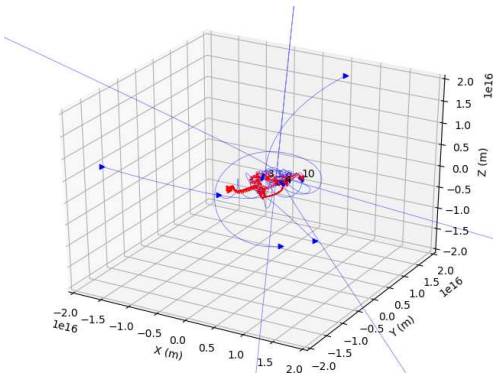

(a) A plot of the positions of the bodies over time. Detected binaries shown in red.

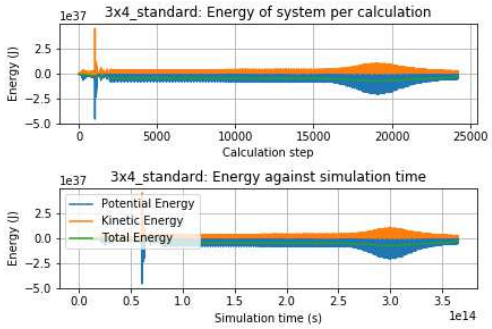

(b) Energy as a function of simulation time and calculation number.

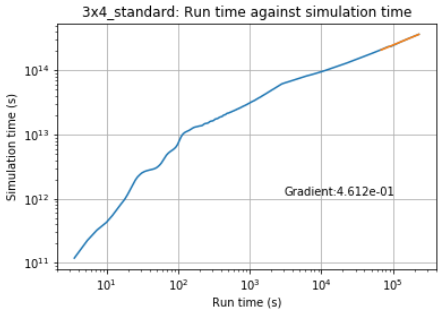

(c) A log log plot of simulation time against runtime. The last half of the data is used to plot the fit (shown in orange).

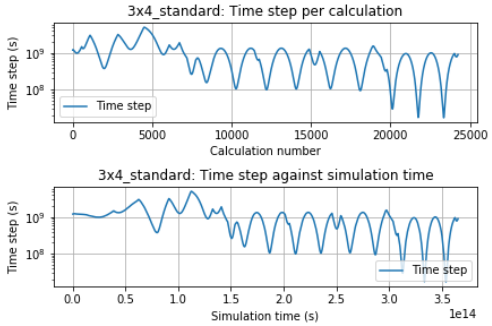

(d) Time step size as a function of simulation time and calculation number.

Figure 3.6: Cluster size = 4, Number of clusters = 3
In this run, an early binary forms from one of the initial clusters. At 3×10^{14} *seconds it interacts with another system breaking apart the binary. A new binary pair is formed which is then ejected as part of a triple system.*

3.3 Binary analysis

The results from 8 runs of a single, five body cluster are used for binary analysis. The random seed was varied for every run but the initial input conditions were kept the same. A total of 39 binaries were identified across the 40 bodies present. This does not account for the fact that some bodies are part of multiple systems, in particular there is a high prevalence of triple systems which account for a significant portion of the 39 binary pairs identified.

In Fig. 3.7, there is a clear division into two main groups with no binaries being detected with a semi-major axis in the range $10^1 - 10^2$au. Currently, it is thought that this division is caused by the detection of both binary and triple systems. The binaries tend to be tightly bound and so are present at $< 10^1$au, whilst triple systems tend to form at larger separations ($> 10^2$au). The gap between the two groupings is likely the region where if a triple is formed, it is close enough to disrupt the central binary pair, making the system unstable and tending to the system breaking apart.

When a triple system is present, the third body will contribute two data points as it interacts with each body in the main binary. This would result in pairs of binaries being detected with very similar potentials and semi-major axis - depending on how tightly bound the central binary is. This can be seen in Fig. 3.7 by the apparent pairing of data points as marked by the circled data points. Although the prevalence of triples initially appears greater than expected, visual observation of the position plots of the systems were checked and corroborated the results from the detection algorithm.

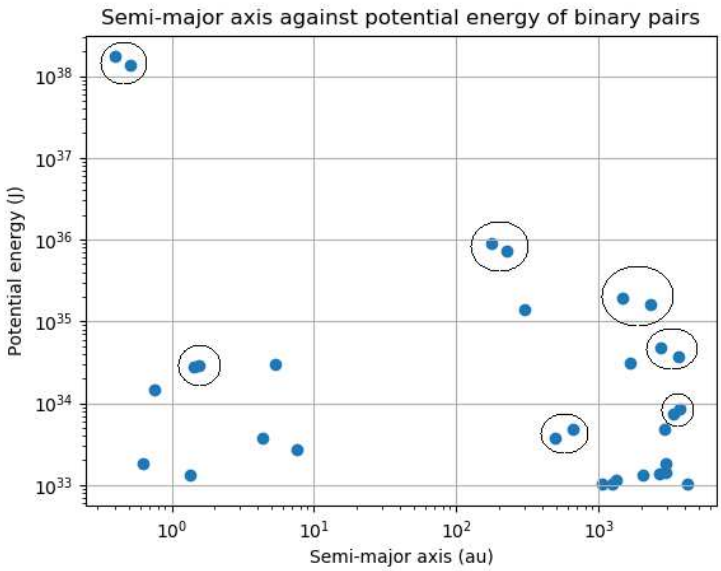

Figure 3.7: Potential energy against semi-major axis for all identified binaries. Duplicate points from triple systems are marked with a circle.

Further investigation into this effect is required, particularly with regards to the width of the theorised "unstable region". Part of this would involve eliminating the double contribution from the triple systems and splitting the data to look more closely at the triple and binaries individually.

To further examine the instability of this region, it would be possible to track the binaries evolution as a function of simulation time. This would provide an indication of the lifetime of triple systems that form within the "unstable region" and whether they tend to break apart completely or interact in such a way as to maintain the system but increase the semi-major axis for the third body. The mass ratios of the binaries was also plotted against both potential energy (Fig. 3.8a) and semi-major axis (Fig. 3.8b). The gap between $a = 10^1 - 10^2$ observed in Fig. 3.7 is also present in Fig. 3.8b. The data points on either side of this region appear to share the same distribution and no overall trend is seen. The distribution of mass ratios as seen in Fig. 3.8c agrees with Duchêne and Kraus 2013 who found that low mass stars have a "mass ratio distribution that is flat or slightly declining towards low-q systems". In this case low mass refers to stars with masses in the range 0.1-0.5 solar masses - in line with the distribution in the simulations (Fig. 3.8d).

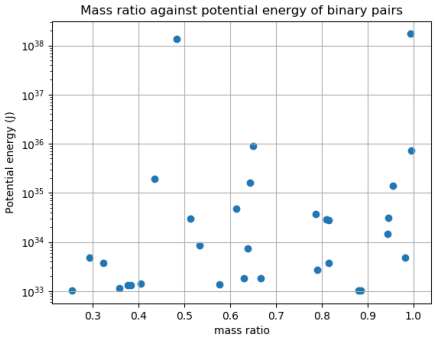

(a) Mass ratio against potential energy.

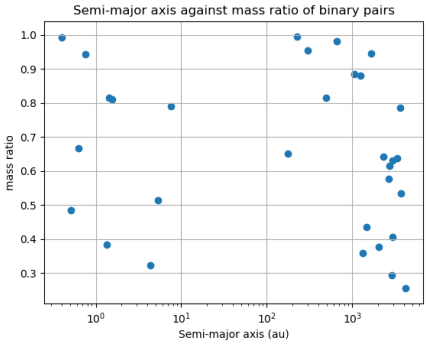

(b) Semi-major axis against mass ratio.

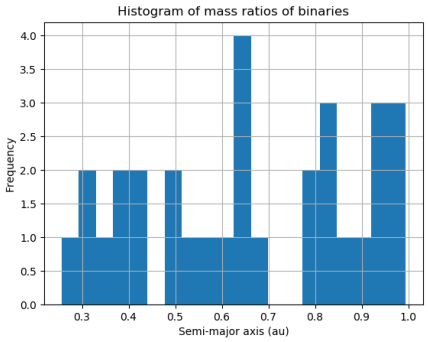

(c) Histogram of mass ratios of binaries. A slight trend to higher mass ratios is seen but more data is needed to confirm this.

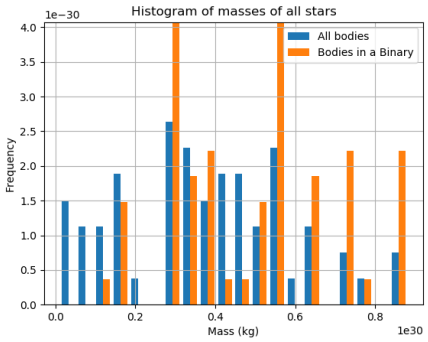

(d) Histogram of masses of all the stars and those stars present in binary systems.

Figure 3.8: Plots involving the mass ratio of the detected binary systems.

Chapter 4

Analysis and conclusions

4.1 Errors and problems

4.1.1 Dynamic time stepping

One of the major drawbacks of the current method of running the simulations is that whilst the addition of dynamic time stepping allows for systems to evolve much faster in general, once any given body within the simulation has a high acceleration, the entire program must slow down to a time step suitable for maintaining the accuracy of the fast moving body.

This can be seen in Figs: 3.2d, 3.3d, 3.4d, 2.4d, 3.5d, 3.6d, where there is initial, chaotic, changing of the time step - indicating multiple interactions but maintaining a relatively large average time step. However, the fact that binaries form relatively early from a single cluster self-interacting, and that tight binaries tend to have greater accelerations, the formation of a single tight binary forces a small time step and limits the progression of the system from that point on wards.

A possible solution to this is to apply a combination of nearest-neighbour detection (Aarseth 2003) and binary detection. At specified intervals, the simulation can be checked for binary pairs above a threshold potential energy. These can then be modelled as a single body if they are not interacting with any other objects. This new "binary object" can then check with a nearest-neighbour code whether it is within a specified interaction distance of other bodies. If it is not and the binary is isolated, it can safely be modelled as a single particle as without any outside force, the binary system should be stable (The stability of these binaries is demonstrated by the tending of the Δt graphs to a constant, oscillating value consistent with the binary.

In the case where the binary is within interaction distance of another body, the binary can again be modelled as the two individual bodies, resulting in a slower simulation time step but maintaining the ability for interactions to change/form/breakup binary pairs. In the case of an ejected binary (the most likely outcome for a single cluster as seen in the test of a five body cluster), the simulation will no longer slow down unnecessarily and further interactions over a larger time scale will occur in significantly less real world run time.

4.1.2 Reliability of N-body simulations

In general, the strength of N-body simulations lies in the fact that with a large enough sample size, the statistical results hold up well to comparison against real systems - individual simulations however do not (Boekholt and Portegies Zwart 2015). Given the time and computational limitations of the project, there is limited access to repeat data. Moving forward with this project, a goal would be to run repeats of the current simulation set-ups to ensure the current results hold over many repetitions. Code is in place for this to be achieved as the seed used for the random aspects of the initial conditions generation is included in the initial conditions file. It is a simple matter to run multiple simulations of the same conditions with a different initial seed (as in the multiple runs of a single cluster) in order to determine the results of an ensemble of runs.

4.2 Conclusions

The initial aims of the project were to design and create the following in order to investigate the effect of a filamentary structure on the formation of binary and triple systems:

- Initial conditions modelled after filaments observed in a GMC
- An N-body integrator
- Automated binary system detection and classification

The generation of randomised clusters of bound stars involved both scaling the positions of the stars within the cluster to proportions similar to those observed by (André 2010), and scaling the velocities such that the system is initially in virial equilibrium (Eq. (1.1). The scaling of the velocities was determined to be accurate through the testing of a simple binary system with random initial velocities. After scaling the system was evolved for several orbital periods and the system is shown to be bound (2.2a, 2.1a).

This testing also provided insight into the rates of formation of binary systems from single, isolated clusters (3.2, 3.3, 3.4). It was found that in every test of an initially bound cluster, at least one binary system was formed through dynamic interaction. The presence of triple systems was also found but due to the limitations imposed by the increasingly small time step that tight binaries impose, further evolution of these systems was restricted and so the stability of the triple systems has not been determined.

The generation of the filaments (2.5) was quantified as being successful when the filament was scaled such that each cluster was isolated enough to complete an initial interaction - tending to form a binary in the process - but also close enough to neighbouring clusters such that cluster-cluster interaction was observed (3.5, 3.6).

The choice of N-body integrator was made in part by the requirement of having a symplectic integration scheme whilst keeping computation time down for each time step calculation. A direct comparison of the Euler and Velocity-Verlet schemes was made and after analysis of a simple binary system, the Verlet scheme was chosen (2.1).

The automated binary detection is limited in that it has no time sensitivity. The algorithm evaluates only a single given time step and calculates the binaries present only at that time. Because of this, there is not indication of stability of a given binary other than manually checking at regular intervals and comparing the results. This also introduces a source of error for determining triple systems as they tend to be more unstable and are more weakly bound than isolated binaries.

The investigation into the effect of a filamentary structure is limited due in part to a lack of repeat simulations in order to create an ensemble of results with similar initial conditions - without this ensemble, an N-body integrator is inherently unreliable and single runs should not be considered in too much depth.

The extent of the filaments generated is also limited by the number of bodies present in the simulation. Due to problems arising from running long simulations, a maximum of 12 bodies in a single run was imposed. This greatly reduced run time from the initial goal of 25 bodies at the expense of a loss of large filaments being investigated.

The mass ratio of detected binaries is inline with the results from Duchêne and Kraus 2013 and follows a slight declining trend towards low mass ratio systems (Fig. 3.8c. This is also seen in Fig. 3.8d where the mass distribution for the stars in binaries is similar to the initial mass distribution.

Overall, the project was successful in creating and modelling pre-stellar cores in clusters of 3-5 stars; attempts to investigate the effect the presence of multiple clusters in a filament would have on the individual clusters were made but further investigation is required. The framework of code has been set-up in a way to allow for future investigations to be easily implemented as there is full control over conditions such as; the mass distribution, body and cluster positions and velocities, and the overall filament structure. In addition, the binary detection is designed such that it should be unaffected by scaling to larger simulations.

References

Aarseth, Sverre J. (2003). "Neighbour treatments". In: *Gravitational N-Body Simulations: Tools and Algorithms*. Cambridge Monographs on Mathematical Physics. Cambridge University Press, pp. 32–50. DOI: 10.1017/CBO9780511535246.004.

André, Ph. et al. (2010). "From filamentary clouds to prestellar cores to the stellar IMF: Initial highlights from the Herschel Gould Belt Survey". In: *Astronomy and Astrophysics* 518.L102.

Athanassoula, E. et al. (2000). "Optimal softening for force calculations in collisionless N-body simulations". In: *Monthly Notices of the Royal Astronomical Society* 314(3), pp. 475–488.

Bate, Matthew R., Ian A. Bonnell, and Nigel M. Price (1995). "Modelling accretion in protobinary systems". In: *Monthly Notices of the Royal Astronomical Society* 277.2, pp. 362–376. ISSN: 0035-8711. DOI: 10.1093/mnras/277.2.362. URL: https://doi.org/10.1093/mnras/277.2.362.

Batten, A. H. (1973). *Binary and multiple systems of stars*. Pergamon.

Boekholt, T. and S. Portegies Zwart (2015). "On the reliability of N-body simulations". In: *Computational Astrophysics and Cosmology* 2, 2, p. 2. DOI: 10.1186/s40668-014-0005-3. arXiv: 1411.6671.

Duchêne, Gaspard and Adam Kraus (2013). "Stellar Multiplicity". In: *Annual Review of Astronomy and Astrophysics* 51.1, pp. 269–310. DOI: 10.1146/annurev-astro-081710-102602.

Goodwin, S.P. (2007). "The relationship between the prestellar core mass function and the stellar initial mass function". In: *Astronomy & Astrophysics* 477(3), pp. 823–827.

Jeans, C. J (1919). "The origin of binary systems". In: *Monthly Notices of the Royal Astronomical Society* 79(6), pp. 408–416.

Lada, C. J. and E. A. Lada (2003). "Embedded Clusters in Molecular Clouds". In: *Annual Review of Astronomy and Astrophysics* 41(1), pp. 57–115.

Shu, F (1987). "Star Formation In Molecular Clouds: Observation And Theory". In: *Annual Review of Astronomy and Astrophysics* 25(1), pp. 23–81.

Tohline, J.E. (2002). "The Origin of Binary Stars". In: *Annual Review of Astronomy and Astrophysics* 40(1), pp. 349–385.

Turner, J.A. (1995). "Binary star formation: gravitational fragmentation followed by capture". In: *Monthly Notices of the Royal Astronomical Society* 277(2), pp. 705–726.